ELSEVIER

Journal of Alloys and Compounds 434–435 (2007) 415–419

Journal of ALLOYS AND COMPOUNDS

www.elsevier.com/locate/jallcom

Synthesis and characterization of nanocrystalline FeNiZrB developed by mechanical alloying

J.J. Suñol [a,*], A. González [a], J. Bonastre [a], M.T. Clavaguera-Mora [b], B. Arcondo [c]

[a] *University of Girona, EPS, Campus Montilivi s/n, Girona 17071, Spain*
[b] *University of Autónoma Barcelona, Fac Ciencias, Grup Fisica Materials 1, Bellaterra 08193, Spain*
[c] *University of Buenos Aires, Fac Ingn, Lab Solidos Amorfos, Buenos Aires, DF RA-1063, Argentina*

Available online 16 October 2006

Abstract

Mechanical alloying (MA) represents a non-expensive versatile route able to produce equilibrium as well as non-equilibrium materials including amorphous, nanostructured composites, and extended solid solution systems. In this work, two nanocrystalline alloys: $Fe_{71}Ni_{14}Zr_6B_9$ (A) and $Fe_{60}Ni_{14}Zr_6B_{20}$ (B) were developed. The as milled (80 h) alloy consisted primarily of metastable BCC-(Fe, Ni) nanocrystals (6–10 nm). The apparent activation values obtained are 3.2 ± 0.1 and 2.6 ± 0.1 eV for alloys A and B, respectively. The structural behaviour determined by X-ray diffraction and Mössbauer spectroscopy indicates that the thermally induced crystallization processes are related to the crystalline growth of the BCC-(Fe, Ni) phase and to formation of FCC-(Fe, Ni) and (Fe, Ni)$_2$-B phases.

Keywords: Mechanical alloying; Nanocrystalline materials; Fe based materials

1. Introduction

In the last decades, the nanocrystalline Fe based materials have attracted considerable interest because of their specific physical properties, differing from those of polycrystalline and amorphous materials of the same chemical composition [1,2]. A wide variety of techniques are being used to synthesize nanostructured metallic materials including inert gas condensation [3], electrodeposition [4], crystallization of amorphous phases [5], sputtering [6] or mechanical alloying [7].

Our experiments are based in mechanical alloying (MA) as an alternative technique to obtain metastable materials in powdered form. This technique has been described as a complex process that involves deformation, fragmentation, cold solder and microdifusion in a highly energetic grinding media. The milled alloys present a similar nanocrystalline structure as quenched ribbons after annealing at elevated temperatures [8]. However, the magnetic properties of the mechanically attrited materials are inferior to rapidly quenched materials. Recently, melt-spun Fe–X–B (X = Nb, Zr) based alloys with crystallite sizes less than 100 nm, have attracted attention due to their magnetic properties such as effective permeability and saturation magnetic flux density [9–11]. However, the magnetic properties of the mechanically attrited materials are inferior to rapidly quenched materials [12,13] because of the stress generated by the process. Nevertheless, the use of melt-spun materials in power transformers and other energy-conversion devices has been limited by their small thickness [14]. It has also, over the years, proved that MA to be superior to rapid solidification processing as a non-equilibrium processing tool [15].

In this work we have investigated the structural, compositional and thermal evolution of the alloy structure during the milling process of two Fe–Ni–Zr–B alloys. The formation of non-soft magnetic compounds as Fe_2B limits their thermal stability.

2. Experimental

Mechanical alloying was carried out in a planetary high-energy ball mill (Fritsch Pulverisette P7) starting from pure elements and compound powders (Fe of 99.7% purity, with a particle size under 10 μm; B of 99.6% purity, with a particle size 50 μm and Ni_7Zr_3 of 99% purity, with a particle size under 100 μm). A ball-to-powder mass ratio of 5:1 was used. Oxidation was reduced by milling in argon atmosphere. The milling process was performed at a speed of 600 rpm for 10, 20, 40 and 80 h using stainless steel balls and a vial with a ball-to-powder mass ratio of 5:1. The alloys produced and analyzed were: $Fe_{71}Ni_{14}Zr_6B_9$ and $Fe_{60}Ni_{14}Zr_6B_{20}$, labelled as A and B, respectively.

* Corresponding author. Fax: +34 972418098.
E-mail address: joanjosep.sunyol@udg.es (J.J. Suñol).

0925-8388/$ – see front matter © 2006 Elsevier B.V. All rights reserved.
doi:10.1016/j.jallcom.2006.08.319

The sample thermal characterization was carried out by differential scanning calorimetry (DSC) under an argon atmosphere in a DSC30 equipment of Mettler-Toledo. The morphology and composition study was performed by scanning electron microscopy (SEM) in a DSM960 A Zeiss equipment with energy dispersive X-ray microanalysis (EDX) and by induced coupled plasma (ICP) in a Liberty-RL ICP Varian equipment. X-ray diffraction (XRD) patterns were carried out in a D-500 Siemens equipment using Cu Kα radiation. Mössbauer characterization of Fe environments was performed at room temperature with a constant acceleration spectrometer employing a ^{57}Co (Rh) source. The spectra were fitted employing the Normos-Dist program by Brand [16] assuming that Fe environments are involved in Fe–Ni solid solutions. In addition one or more discrete environments are proposed. The isomer shift (δ) values are reported relative to BCC-Fe absorber.

3. Results and discussion

The topology of the powders was followed by SEM. As an example Fig. 1 shows micrographs of alloy A after 80 h of milling. As increasing the milling time, the average grain size diminishes, but high agglomerates were produced with smooth appearance. EDX microanalysis of localized zones shows also the oxygen contamination due to the oxide formation. The inductive coupled plasma (ICP) and energy-dispersive X-ray (EDX) results show slight (<2.0 at.%) contamination from the milling tools (Fe, Ni and Cr) and from the atmosphere (oxygen). Detected contamination increases with the milling time.

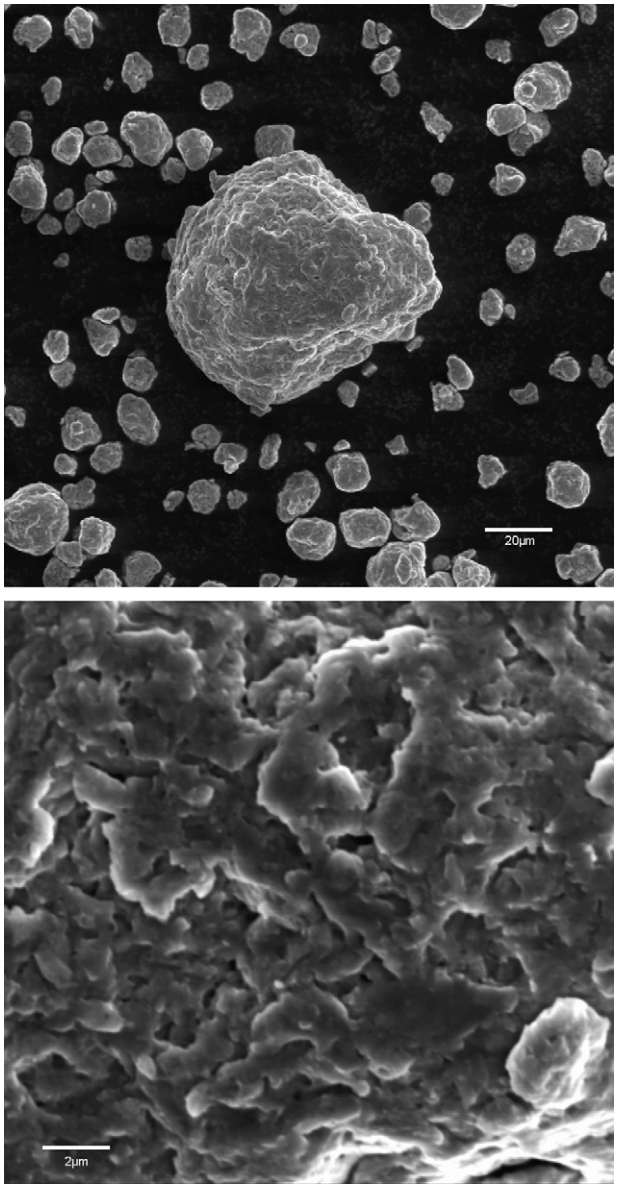

Fig. 1. SEM micrographs of alloy A milled during 80 h.

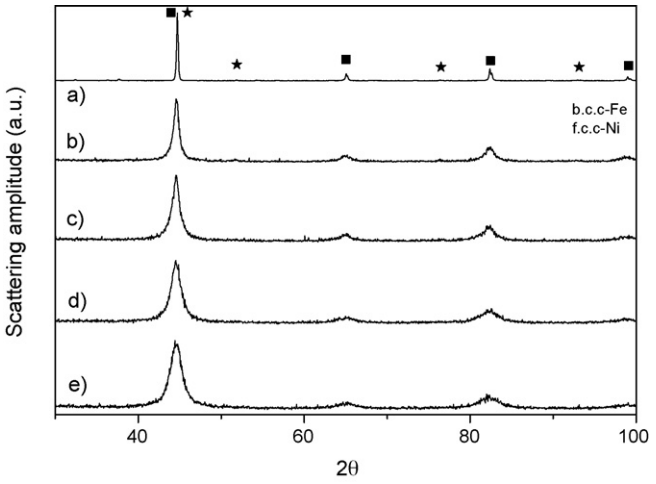

Fig. 2. X-ray diffraction patterns of alloy A milled during: (a) 0 h, (b) 10 h, (c) 20 h, (d) 40 h and (e) 80 h.

The formation of the nanocrystalline structure during mechanical alloying was followed by X-ray diffraction. Figs. 2 and 3 correspond to the XRD spectra of alloys A and B, respectively. As increasing the milling time, the BCC iron peaks broaden and their intensity decrease while the FCC nickel peaks disappear. The resultant diffraction spectra were corrected from the $K_{\alpha 2}$ effects prior to the collection of peak location and full width at half-maximum data. Following instrumental broadening correction, the data were separated into broadening components attributed to fine crystallite size and to plastic strain using a Warren–Averbach method employed by different authors [17,18]. The lattice strain observed, between 0.2 and 0.8%, is in accordance with typical values of distorted lattices but in contrast

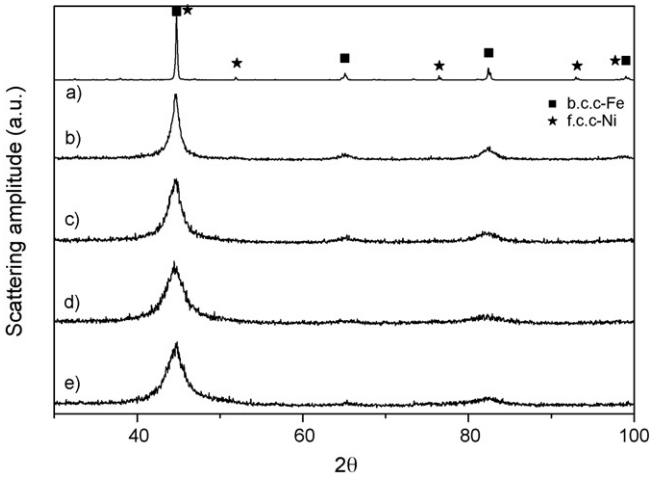

Fig. 3. X-ray diffraction patterns of alloy B milled during: (a) 0 h, (b) 10 h, (c) 20 h, (d) 40 h and (e) 80 h.

with the grain size, we found that the lattice strain increase as a function of the milling time. A maximum value of above 1% was reached in multicomponent Fe–Co–Ni–Zr–B alloys [19]. The nanocrystallites formed after 80 h of milling were about 10 and 6 nm average size for alloys A and B, respectively. Usually Ni enhances the amorphyzation process [20,21].

For each milled powdered sample, lattice parameter values were calculated from the high angle peak positions and were effectively corrected for systematic error due to displacement of the powder sample from the diffractometer analysis using the procedure described in Ref. [22]. The lattice parameter, after 80 h MA, are higher, 0.2875(4) and 0.2871(4), than that of the pure bcc Fe structure indicating the presence of other elements in solid solution. A value of 0.2879 was found in $Fe_{70}Zr_{10}B_{20}$ powder milled [23]. Furthermore, the lattice parameter increases with increasing milling time. However, XRD analysis shows that nanocrystallite size and lattice parameter becomes nearly stable after 40 h MA.

Thermal study was performed by differential scanning calorimetry (DSC). Fig. 4 shows constant heating rate ($\beta = 10$ K/min) DSC curves corresponding to alloys A and B respectively after 80 h of milling. At low temperature, about 390 K, an exothermal process begins. This is a signature of recovery of stress, that is, mainly deformation energy stored during the milling process. As increasing the temperature, one or two crystallization processes appear related with the crystal growth, reordering and formation of the crystalline phases. The shape of the DSC scans of alloy A milled for 10–80 h are similar and it is was also found in other Fe–Ni based alloys obtained by MA [24,25]. The exothermic peaks are wider and less sharp

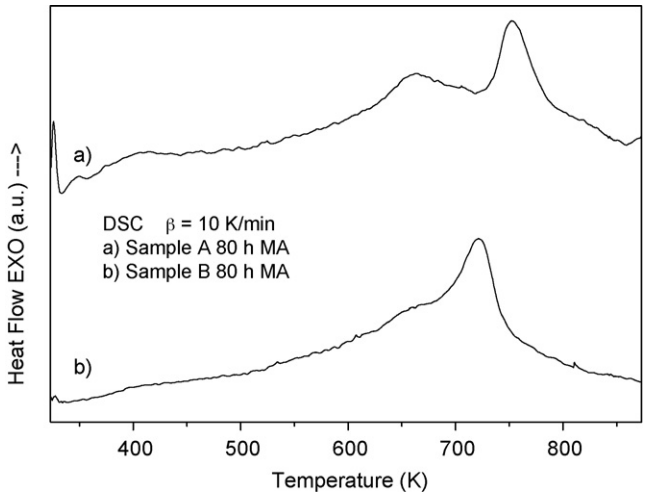

Fig. 4. DSC at constant heating rate ($\beta = 10$ K/min) curves corresponding to alloys A and B after 80 h of milling.

for powder than those for melt-spun or bulk materials. This is due to the fat that the powder has a particle size distribution [19,21]. Furthermore, as increasing the milling time the recovery becomes more energetic.

The apparent activation energy, E, for the main crystallization process of alloys milled 80 h can be evaluated using the Kissinger equation: $\ln(\beta/T_p^2)$ versus $1/T_p$ with β the heating rate and T_p the peak temperature [26]. The values obtained are 3.2 ± 0.1 and 2.6 ± 0.1 eV for alloys A and B, respectively. Similar energy values were found for $Fe_{87}Zr_7B_6$, $Fe_{86}Zr_7B_6Cu_1$ [27], $Fe_{85.5}Zr_4Nb_4B_{5.5}Al_1$ [28] and multi-component FeNiZrB [19].

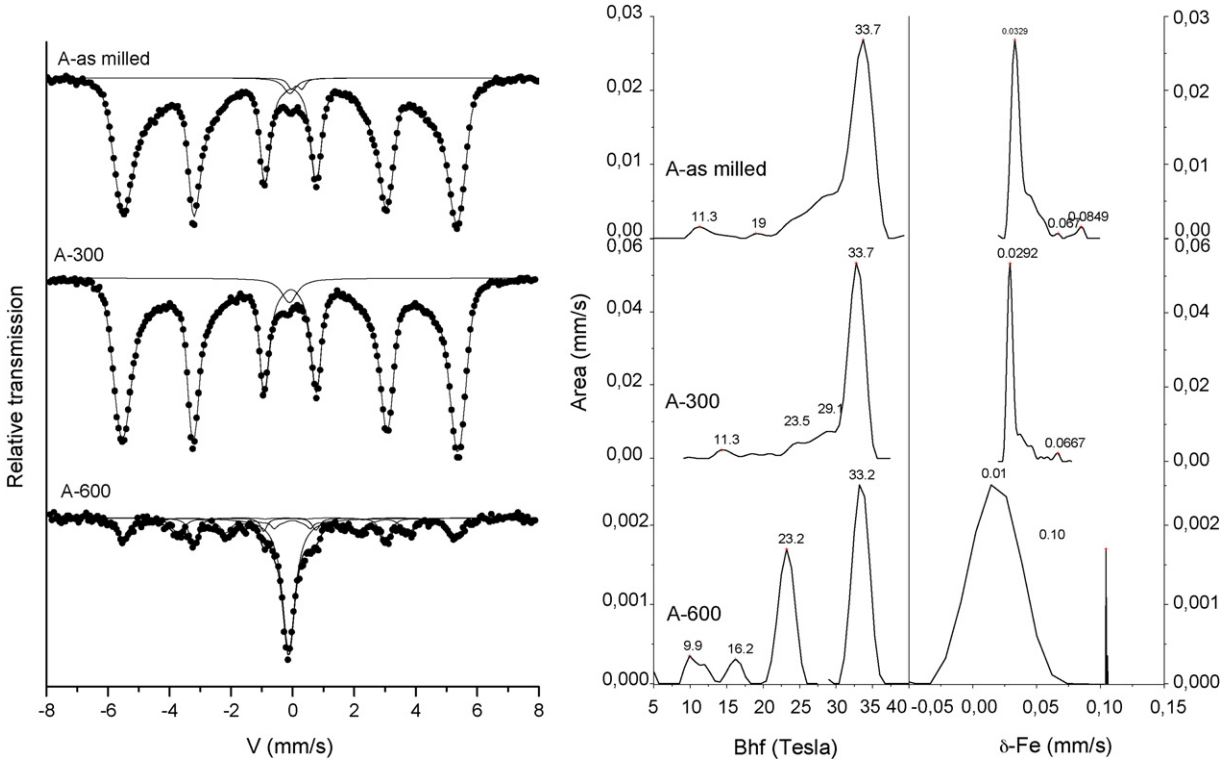

Fig. 5. Mössbauer spectra and distribution of hyperfine magnetic fields (Bhf) of alloy A as milled for 80 h and after thermal treatments during 1 h at 300 and 600 °C.

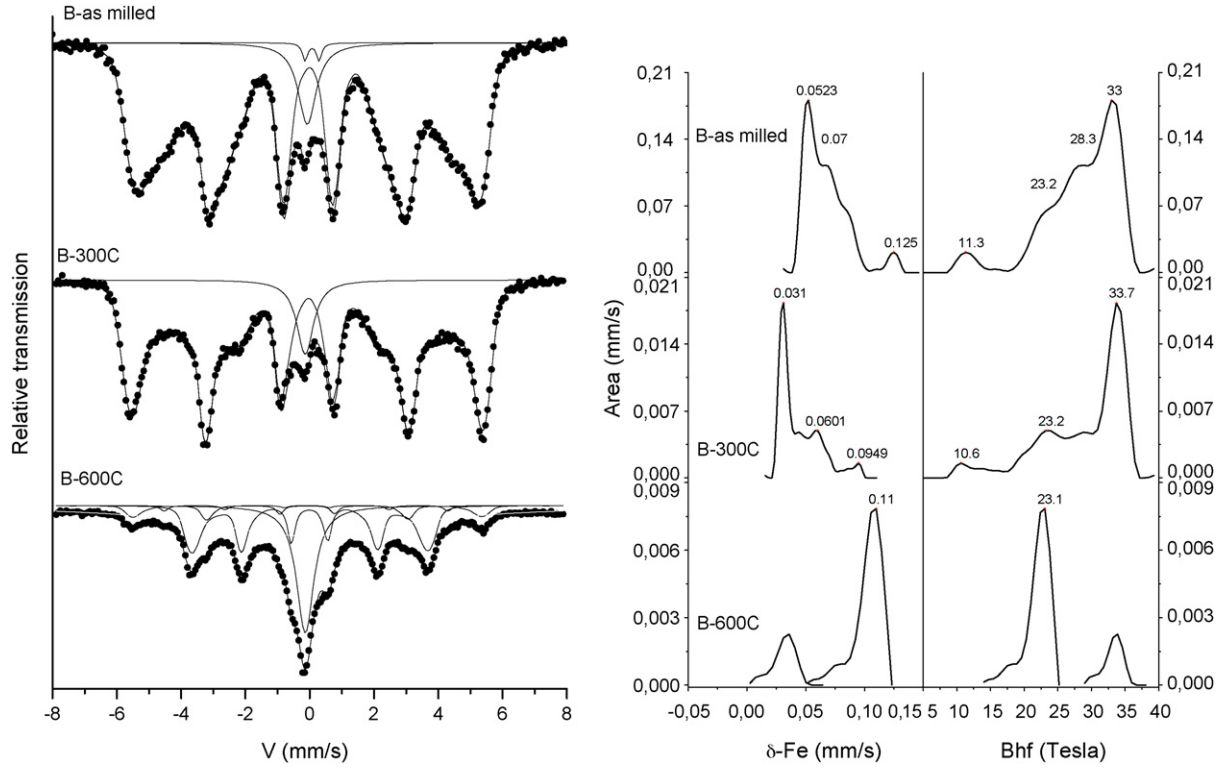

Fig. 6. Mössbauer spectra and distribution of hyperfine magnetic fields (Bhf) of alloy B as milled for 80 h and after thermal treatments during 1 h at 300 and 600 °C.

The highest activation energy and characteristic temperature of crystallization indicates that higher thermal stability of alloy A (which corresponds to a higher Fe/B ratio). Furthermore, it is important to detect the formation of non-soft magnetic compounds as Fe_2B to design annealing treatments of these alloys.

Transmission Mössbauer experiments were performed at room temperature on samples milled for 80 h and isothermally treated at 300 and 600 °C for 1 h (Figs. 5 and 6). The samples are inhomogeneous as revealed by broad hyperfine field distributions, the same result was found in multicomponent Fe–Ni–Zr–B [23]. For both alloy compositions the BCC-Fe based solid solution was formed preferably.

In as milled samples, before thermal annealing, the Mössbauer spectra were fitted employing a hyperfine magnetic field (Bhf) distribution corresponding to solid solutions of one or more elements in the BCC-Fe phase. In alloy A the main contribution (97% of the spectral area) is a Bhf distribution corresponding to BCC-Fe–Ni based solid solution with a $Bhf_{peak\ value} = 33.7$ T and $\delta_{peak\ value} = 0.03$ mm/s. The resultant quadrupole splitting is $\Delta = -0.02$ mm/s. In alloy B a very wide Bhf distribution (93 area%) denotes an increasing disorder, involving not only Fe and Ni but also B or Zr atoms. Hyperfine parameters $Bhf_{peak\ value} = 33$ T, $\delta_{peak\ value} = 0.05$ mm/s and $\Delta = -0.01$ mm/s correspond to a BCC-Fe rich phase. Ni increases the hyperfine field and Zr reduces it [23]. In both spectra, a less important contribution to Bhf about 12 T can be related to disordered FeZrB environments [29]. In addition, two weak paramagnetic interactions are observed, one of them, a singlet, corresponds to a low moment (LM) Fe rich FCC phase named antitaenite [30,31] with $\delta = 0.02$ mm/s, the other (1% area) is a doublet which hyperfine parameters are $\delta \approx 0.21$ mm/s and $\Delta \approx 0.40$ mm/s.

Mössbauer spectra obtained from samples A and B previously heated at 300 °C indicate a relief of internal stresses on both samples whereas the growing of a (Fe, Ni) boride contribution to the Bhf distribution (Bhf ≈ 23.2 T) was additionally observed in sample B. The spectra of both samples heated at 600 °C show the crystallization of a low moment iron rich paramagnetic antitaenite (45% area in A and 37% area in B) with $\delta = -0.02$ mm/s. This transformation, consequence of a thermally activated diffusion process, takes place favored by the annealing conditions.

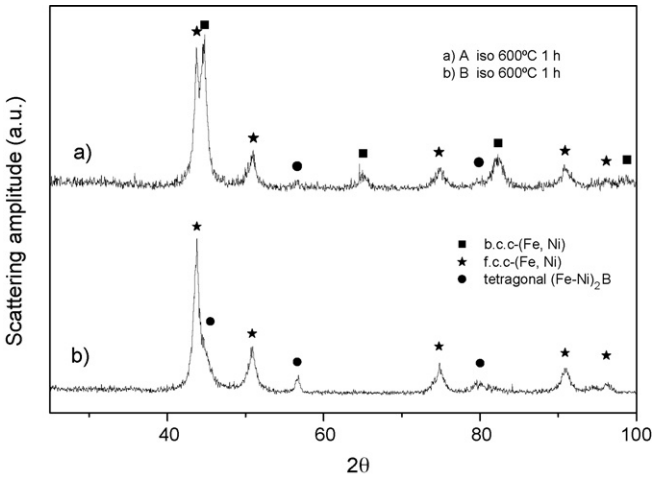

Fig. 7. X-Ray diffraction peaks of alloys A and B milled during 80 h after annealing at 600 °C.

Ferromagnetic BCC-(Fe, Ni) (28% area in A and 12% area in B) with $\langle Bhf \rangle = 33.5$ T, $\langle \delta \rangle = 0.02$ mm/s and $\Delta = 0.00$ mm/s and $(Fe, Ni)_2B$ (25% area in A and 48% area in B) with $\langle Bhf \rangle = 21$ T, $\langle \delta \rangle = 0.10$ mm/s and $\Delta = 0.02$ mm/s are additionally observed. The microstructure evolution was followed by X-ray diffraction (XRD). As shown in Fig. 7, the crystallization process is related to the crystalline growth of the BCC-(Fe, Ni) phase and to formation of FCC-(Fe, Ni) and the $(Fe, Ni)_2$-B phases, in agreement with Mössbauer results.

4. Conclusions

Two nanocrystalline alloys (6–10 nm), $Fe_{71}Ni_{14}Zr_6B_9$ and $Fe_{60}Ni_{14}Zr_6B_{20}$, have been produced by mechanical alloying after milling during 80 h. The higher thermal stability of alloy with the highest Fe/B ratio is determined by activation energy and characteristic temperature of the main crystallization process values.

Transmission Mössbauer experiments performed at room temperature on samples milled for 80 h confirms the formation of solid solutions of one or more elements in the BCC-Fe phase. Spectra after annealing at 300 °C indicate a relief of internal stresses on both samples whereas the growing of a (Fe, Ni) boride contribution to the Bhf distribution ($Bhf \approx 23.2$ T) was observed in sample with more boron content. The spectra of both samples annealed at 600 °C show the crystallization of a low moment iron rich paramagnetic antitaenite (45% area in A and 37% area in B) related to a thermally activated diffusion process. Ferromagnetic BCC-(Fe, Ni) (28% area in A and 12% area in B) and the non soft magnetic $(Fe, Ni)_2B$ (25% area in A and 48% area in B) are additionally observed.

Acknowledgements

Financial support from MICYT (project No. MAT2003-08271) and DURSI (project 2005SGR-00201) is acknowledged. A.G. also acknowledges an UdG fellowship and J.B. and FPI Spanish fellowship.

References

[1] M.E. McHenry, M.A. Willard, D.E. Laughlin, Prog. Mater. Sci. 44 (1999) 291.
[2] J.S. Garitaonandia, P. Gorria, L. Fernández Barquín, J.M. Barandiarán, Phys. Rev. B 26 (9) (2000) 6150.
[3] G.W. Nieman, J.R. Weertman, R.W. Siegel, Scripta Metall. 23 (12) (1989) 2013–2018.
[4] C. Cheung, G. Palumbo, U. Erb, Scripta Metall. Mater. 31 (1994) 735–740.
[5] A. Makino, A. Inoue, T. Masumoto, Mater. Trans. JIM 36 (7) (1995) 924–938.
[6] H. Hahn, R.S. Averback, J. Appl. Phys. 67 (2) (1990) 228–239.
[7] A.R. Yavari, Mater. Trans. JIM 36 (2) (1995) 228–239.
[8] J. Nogues, K.V. Rao, A. Inoue, K. Suzuki, Nanostruct. Mater. 5 (1995) 281.
[9] A. Makino, T. Hatanai, A. Inoue, T. Matsumoto, Mater. Sci. Eng. A 226 (1997) 594.
[10] M. Kopcewicz, A. Grabias, D.L. Williamson, J. Appl. Phys. 82 (1997) 1747.
[11] C.A.C. Souza, M.F. de Oliveira, J.E. May, W.J. Botta, N.A. Mariano, S.E. Kuri, C.S. Kiminami, J. Non-Cryst. Solids 273 (2000) 282.
[12] M.M. Raja, K. Chattopadhvav, B. Majumdar, A. Naravanasamy, J. Alloys Compd. 297 (2000) 199–205.
[13] K. Suzuki, J.M. Cadogan, J. Appl. Phys. 87 (2000) 7097.
[14] R.B. Schwarz, T.D. Shen, U. Harms, T. Lillo, J. Magn. Magn. Mater. 283 (2004) 223–230.
[15] B.S. Murty, S. Ranganathan, Int. Mater. Rev. 43 (1998) 101–141.
[16] R.A. Brand, Normos Program, Internal Report, Angewandte Physik, Universitat Duisburg (1987).
[17] H.J. Fecht, E. Hellstern, Z. Fu, W.L. Johnson, Metall. Trans. A 21 (1990) 2333.
[18] R.J. Pérez, B. Huang, P.J. Crawford, A.A. Sharif, E.J. Lavernia, Mater. Sci. Eng. A 204 (1995) 217.
[19] Y.J. Liu, I.T.H. Chang, Acta Mater. 50 (2002) 2747–2760.
[20] Y.J. Liu, I.T.H. Chang, Mater. Sci. Eng. A 325 (2002) 25–30.
[21] J.J. Suñol, N. Clavaguera, M.T. Clavaguera-Mora, J. Non-Cryst. Solids 287 (2001) 114–119.
[22] B.D. Cullity, Elements of X-Ray Diffraction, Addison–Wesley, Reading, MA, 1978, p. 359.
[23] A. Grabias, M. kopcewicz, D. Oleszak, J. Alloys Compd. 339 (2002) 221–229.
[24] J.J. Suñol, T. Pradell, N. Clavaguera, M.T. Clavaguera-Mora, Phil. Mag. 83 (20) (2003) 2323–2342.
[25] T. Pradell, J.J. Suñol, N. Clavaguera, M.T. Clavaguera-Mora, J. Non-Cryst. Solids 276 (2000) 113–121.
[26] H. Kissinger, Anal. Chem. 29 (1957) 1702.
[27] P. Duhaj, I. Matko, P. Svec, J. Sitek, D. Janickovic, Mater. Sci. Eng. B 39 (1996) 208.
[28] A.-H. Mansour, J. Barry, J. Mater. Sci. Lett. 17 (1998) 1127.
[29] R. Pizarro, J.S. Garitaonandia, F. Plazaola, J.M. Barandiarán, J.M. Greneche, J. Phys. Condens. Matter 12 (2000) 3101–3112.
[30] D.G. Rancourt, K. Lagarec, A. Densmore, R.A. Dunlap, J.I. Goldstein, R.J. Reisener, R.B. Scorzelli, J. Magn. Magn. Mater. 191 (1999) 255–260.
[31] Y.A. Abdu, H. Annersten, T. Ericsson, P. Nordblad, J. Magn. Magn. Mater. 280 (2004) 243–250.